Magnetic anisotropies in body-centered-cubic cobalt films

S. Subramanian, X. Liu, R. L. Stamps, and R. Sooryakumar
Department of Physics, The Ohio State University, Columbus, Ohio 43210

G. A. Prinz
Naval Research Laboratory, Washington, D.C. 20375
(Received 7 March 1995)

The origin of magnetic anisotropies in thin bcc cobalt films is investigated using Brillouin light scattering. The in-plane directional and wave-vector dependence of surface and bulk magnon frequencies in (110) and (001) oriented films indicate a twofold anisotropy in these cubic ferromagnets with the easy axis of magnetization lying in plane along [001] and [100], respectively. Using elastic constants determined from phonon dispersion measurements, we argue that the observed uniaxial anisotropy can be largely accounted for by magnetoelastic interactions driven by lattice mismatch at the film/substrate interface. The easy axis is also evident by the transformation of the surface spin wave into the $n=0$ bulk magnon when the magnon wave vector lies parallel to the spontaneous (easy) axis of magnetization.

I. INTRODUCTION

Recent advances in thin-film growth techniques have enabled new phases of magnetic materials to be stabilized. One such material, cobalt, which naturally occurs in the hexagonal close-packed phase, has been grown in stable fcc and bcc phases as thin supported epitaxial films.[1-3] Studies on some of these phases of Co have concentrated on understanding the observed tendency of the easy axis of magnetization to display a thickness and orientational dependence in laminar and superlattice geometries.[4,5] Phenomenological models have been constructed that attempt to explain the observed anisotropies in terms of magnetocrystalline contributions, magnetoelastic interactions, and strain fields induced by lattice mismatch at the interfaces.[5-10]

Despite the success of some of these models, the specific origins of magnetic anisotropies in thin films are not fully understood. The problem is that the magnetic properties of thin films are very sensitive to the microscopic structure of the interface. Growth conditions, interface strains, roughness, and interdiffusion are all factors which determine magnetic anisotropies. The importance of the interface has been observed for example in thin (<50 Å) films of epitaxial bcc Fe on GaAs, where the roles of the easy and hard magnetization axes reverse at reduced film thickness as a result of anisotropies arising from the interface.[11] Similar effects have also been observed in the case of Fe films (<100 Å) on tungsten substrates.[12,13]

In this paper we examine the character and origin of magnetic anisotropy in the bcc phase of cobalt using Brillouin light scattering from propagating surface and bulk spin-wave excitations. Two bcc Co films of (110) and (001) orientations were stabilized on GaAs substrates as thin films with thicknesses of the order of 200 Å. The two lowest-energy branches of the spin-wave manifold were observed, and an analysis of their dispersion allowed a determination of the anisotropy constants and exchange stiffness constants. Bulk anisotropies are clearly evident in the dispersion of the surface and bulk magnons in films of both orientations. In particular, a large in-plane uniaxial anisotropy contribution is required to account for the measured dependence of the magnon frequency as a function of the in-plane angle in the (110) film. We show, using elastic constants measured on these *same* bcc Co films, that magnetoelastic effects arising from the small lattice mismatch strain largely account for this two-fold anisotropy.

II. EXPERIMENTAL DETAILS

Two bcc cobalt films were grown by molecular-beam-epitaxy techniques as described elsewhere.[3] The films were 202 and 216 Å thick and oriented with the (110) and (001) planes parallel to their respective surfaces. The epilayer thickness was measured during growth to an accuracy of about two monolayers. All films were stabilized on a GaAs substrate that has a lattice mismatch of about 0.25% with the predicted lattice constant of bcc cobalt.[3] The structure of each epilayer was confirmed to be of the bcc phase through x-ray-diffraction and surface-enhanced x-ray-absorption fine-structure (EXAFS) studies.[14] The Brillouin-scattering experiments were performed at room temperature in a backscattering geometry using a six-pass tandem Fabry-Pérot interferometer. *P*-polarized light of up to 150 mW in single-mode 5145- and 6471-Å laser lines was focused onto the sample with a typical sampling time of about 2 h. The angle of incidence of the incident photons θ_i, measured to an accuracy of $\pm 2°$, was used to tune the magnitude of the in-plane magnon wave vector $\mathbf{q}$. The spin-wave excitations were mostly analyzed in the depolarized configuration in order to suppress phonon signals. The direction of $\mathbf{q}$ was systematically varied to lie along various in-plane directions. The in-plane propagation direction labeled by angle ϕ_H (defined below) was measured within an error of $\pm 3°$. A magnetic field was applied

0163-1829/95/52(14)/10194(8)/$06.00

parallel to the layer plane, and spin-wave frequencies were measured for **q** *always* propagating perpendicular to the applied field.

III. RESULTS

We first briefly review the theory used to fit the Brillouin data, which is discussed in detail in Refs. 15–20 (and references therein). The dominant contributions to the lowest-frequency spin waves in ferromagnets are anisotropies, dipolar magnetic fields, and the external applied field. Frequencies of the surface and bulk modes can be calculated for thin ferromagnetic films including exchange interactions in a continuum limit that is valid for long-wavelength spin-wave excitations. The theory of dipole-exchange behavior begins by solving the equations of motion for the time and spatially varying magnetization **m**. These equations have the form

$$\frac{d}{dt}\vec{m}=\gamma(\vec{m}+\vec{M})\times(\vec{H}_{\text{eff}}+\vec{h}_d)\ , \tag{1}$$

where M is the static magnetization, γ the gyromagnetic ratio, and h_d is the dipolar magnetic field. The effective magnetic field H_{eff} contains the static external magnetic field H, the exchange field, and the net anisotropic fields H_a. The geometry for the spin-wave dispersion calculations was chosen so that the y axis lies normal to both film surfaces and the axis of saturation magnetization lies along the z direction. Specific to our problem is the fact that the anisotropic fields depend upon the crystal orientation.[19,20] We define ϕ_H as the in-plane angle between H and the crystallographic [001] direction for the (110) film, and as the angle between H and the [100] direction for the (001) film. ϕ_H is used to reference the propagation direction of the in-plane magnon wave vector **q**, which always lies normal to H. We define ϕ as the equilibrium angle between the [001] ([100]) and the z axis for the (110) ((001)) films. Since the magnetization does not rotate uniformly with H due to the presence of anisotropy fields within the films, the angle ϕ is computed by numerically minimizing the total energy E with respect to ϕ:

$$E^{(110)}=-HM\cos(\phi_H-\phi)-K_U\cos^2\phi+\frac{K_1}{4}(1+2\sin^2\phi-3\sin^4\phi)\ , \tag{2a}$$

$$E^{(001)}=-HM\cos(\phi_H-\phi)-K_U\cos^2\phi+\frac{K_1}{4}(\sin^2 2\phi)\ . \tag{2b}$$

In the above expressions, we have neglected the out-of-plane anisotropy K_P and the demagnetization energy because the films are magnetized in plane. The effective fields are calculated by expanding the free energy to second order in terms of small fluctuations in the magnetization around the equilibrium direction. The components of dm/dt including exchange for the (110) grown film are

$$\frac{dm_x}{dt}=\gamma\left\{H\cos(\phi_H-\phi)+\left[\frac{2K_1}{M}\right]\{1-[2\sin^2\phi+\tfrac{3}{8}\sin^2(2\phi)]\}+\left[\frac{2K_U}{M}\right](\cos^2\phi)+\frac{2Ak^2}{M}+\left[\frac{2K_P}{M}\right]\right\}m_y-\gamma Mh_y\ , \tag{3a}$$

$$\frac{dm_y}{dt}=-\gamma\left\{H\cos(\phi_H-\phi)+\left[\frac{2K_1}{M}\right]\{1-\tfrac{1}{2}[\sin^2\phi+3\sin^2(2\phi)]\}+\left[\frac{2K_U}{M}\right](1-2\sin^2\phi)+\frac{2Ak^2}{M}\right\}m_x+\gamma Mh_x\ , \tag{3b}$$

while for the (001)-oriented sample dm/dt is given by

$$\frac{dm_x}{dt}=\gamma\left\{H\cos(\phi_H-\phi)+\left[\frac{2K_1}{M}\right][1-\tfrac{1}{2}\sin^2 2\phi]+\left[\frac{2K_U}{M}\right](\cos^2\phi)+\frac{2Ak^2}{M}+\left[\frac{2K_P}{M}\right]\right\}m_y-\gamma Mh_y\ , \tag{4a}$$

$$\frac{dm_y}{dt}=-\gamma\left\{H\cos(\phi_H-\phi)+\left[\frac{2K_1}{M}\right][1-2\sin^2(2\phi)]+\left[\frac{2K_U}{M}\right](1-2\sin^2\phi)+\frac{2Ak^2}{M}\right\}m_x+\gamma Mh_x\ . \tag{4b}$$

In the above equations, A is the exchange energy and h_i's are components of the dipolar fields. The exchange field is proportional to $k^2=q^2+k_y^2$, where q is the in-plane magnon wave vector ($2k_i\sin\theta_i$) and k_y is the wave-vector component perpendicular to the film. K_1 is the first-order fourfold magnetocrystalline anisotropy, and K_U (K_P) is the in-plane (out-of-plane) uniaxial anisotropy. In our convention, $K_U>0$ puts an in-plane easy axis along [001] for the (110) film and [100] for the (001) film. K_P is defined such that $2K_P/M+4\pi M<0$ places an easy axis normal to the film plane, along y. After linearization, the two coupled equations for **m** are solved together with the electromagnetic and exchange boundary conditions.[15] For a given frequency ω and in-plane wave vector **q**, there are six solutions to k_y for the above set of equations. Allowed solutions are a superposition of six partial waves corresponding to the k_y, which must satisfy the exchange and electromagnetic boundary conditions appropriate to the film geometry.

The most striking effect of the dipolar transition is the appearance of a surface localized excitation S, the Damon-Eshbach mode. S is most easily observed in

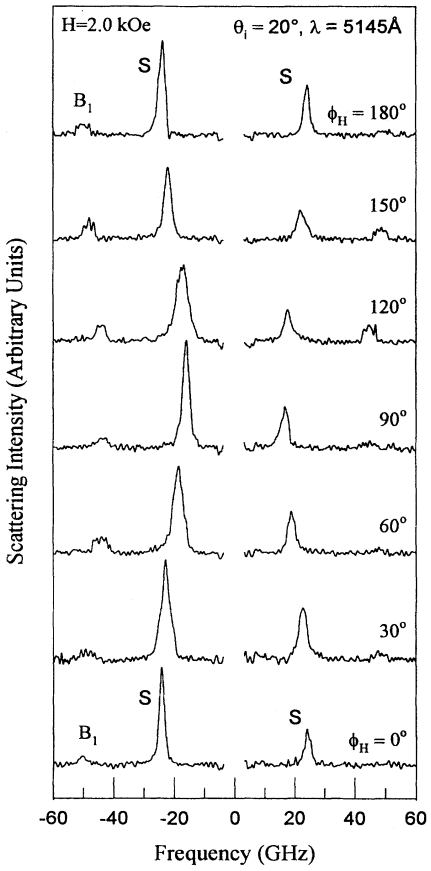

FIG. 1. Depolarized $p \rightarrow s$ Brillouin spectra from (110) grown 202-Å-thick bcc Co film in backscattering, at an angle of incidence $\theta_i = 20°$, external magnetic field $H = 2.0$ kOe, and excitation wavelength $\lambda = 5145$ Å. In all experiments, $\mathbf{q} \perp H$ and hence $\phi_H = 0°$ corresponds to $\mathbf{q}$ propagating along $[\bar{1}10]$ while $\phi_H = 90°$ refers to $\mathbf{q}$ along [001]. S identifies the surface magnon and B_1 the first-order bulk magnon.

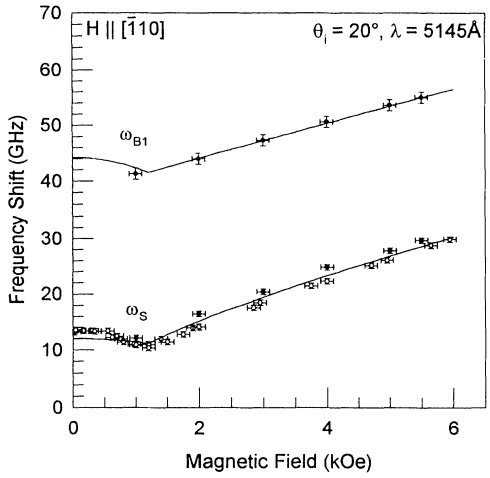

FIG. 2. Magnetic field dependence of the surface (ω_S) and bulk (ω_{B1}) magnon frequencies in the (110)-oriented film. The solid curve through the data is a theoretical fit as discussed in the text. The error bars on ω_S and ω_{B1} are ± 0.5 and ± 1.0 GHz, respectively. The error in the measured magnetic field H is ± 0.1 kOe.

light-scattering experiments because of large dipolar fields near the film surface. Its frequency ω_S also exhibits the interesting property of being largest for propagation perpendicular to M and decreases as $\mathbf{q}$ approaches the magnetization direction. In the latter case, S is no longer localized to the surface, having transformed to the $n = 0$, uniform bulk mode. We find direct evidence in zero applied field for such a transformation of the surface magnon, thus confirming the direction of the easy axis of magnetization.

Figure 1 shows typical Brillouin spectra from the (110)-oriented bcc Co film in the presence of a 2.0-kOe field for excitation at 5145 Å. The spectra were recorded at an angle of incidence $\theta_i = 20°$ with ϕ_H varying systematically between 0° and 180°. The surface (S) and $n = 1$ bulk (B_1) magnons are clearly observed in the spectra. Figure 2 summarizes the field dependence of ω_S and ω_{B1}. The difference between the surface and bulk frequencies is especially sensitive to the exchange constant (A), while the slope of the curves is controlled by the gyromagnetic ratio (γ). The solid curves through the data in Fig. 2 (and Fig. 3) are fits using the theory discussed above.

The two data sets for the surface mode in Fig. 2 (open and solid symbols) were taken using different magnet systems and Fabry-Pérot interferometer calibrations. The slight differences are due to systematic variations in the two experimental setups. The solid line is the best fit made to both data sets. Data for the surface mode in Fig. 2 (open circles) extend all the way down to $H = 0$. The softening of the surface magnon frequency around $H = 1.2 \pm 0.1$ kOe is due to the presence of an in-plane uniaxial anisotropy K_U, which forces the magnetization to lie along [001]. When the external magnetic field exceeds a critical value H_c, the magnetization is pulled into the direction of the field. The frequency of the surface mode has a minimum at H_c and thus provides a measure of K_U since it can be shown that $K_U = (H_c M)/2$. The results of Fig. 3 also indicate the presence of a large in-plane uniaxial anisotropy contribution to the surface and bulk magnon dispersion. The inset shows the behavior of ω_S measured at $\lambda = 6471$ Å for directions $0° \leq \phi_H \leq 360°$ using a 1.2-kOe magnetic field. This is just enough to saturate the magnetization.

On simultaneously fitting the data in Figs. 2 and 3 using the theory described above, we obtained a gyromagnetic ratio $\gamma = 2.02$, exchange constant $A = 1.87 \times 10^{-6}$ erg/cm, $K_P = 8.3 \pm 3 \times 10^5$ erg/cm^3, and $K_1 = 0$ for the (110) film. Independently measured values of $4\pi M$ (13 kG) were used to fit the Brillouin data. The critical field H_c ($= 1.2 \pm 0.1$ kOe) gives $K_U = 6.2 \pm 0.5 \times 10^5$ erg/cm^3 (Table I). This value of K_U was also confirmed by independent dc superconducting quantum interference device (SQUID) measurements. The magnitude of K_U/M largely determines the difference in the magnon frequencies between the easy and hard directions that occur at $\phi_H = 0°$ and 90°. With all other parameters held con-

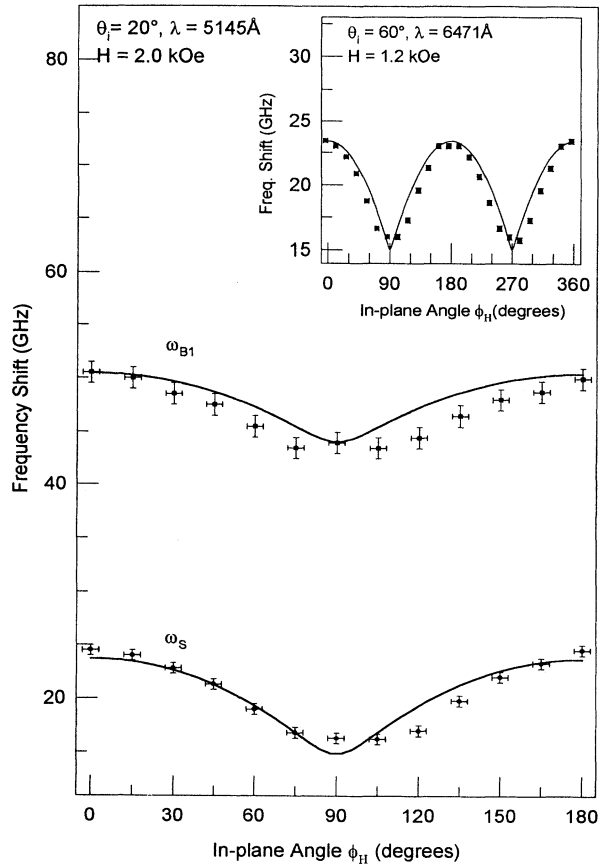

FIG. 3. In-plane magnon dispersion at two different excitation wavelengths from (110)-oriented Co film. The main figure shows spin-wave frequencies measured at 5471 Å, while the inset above shows data recorded with 6471 Å radiation. The solid lines through the surface (ω_S) and bulk (ω_{B1}) magnon frequencies are a fit utilizing parameters discussed in the text. The error bars on ω_S and ω_{B1} are ± 0.5 and ± 1.0 GHz, respectively. The error in ω_S at 6471 Å is ± 0.2 GHz. The angle ϕ_H denotes the in-plane angle between the crystallographic [001] direction and the external magnetic field, and the error in ϕ_H ($\Delta\phi_H$) is $\pm 3°$.

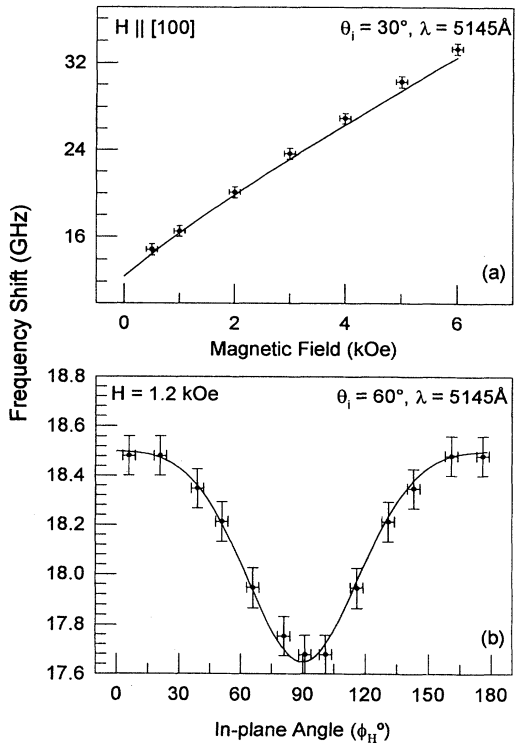

FIG. 4. Field dependence and in-plane dispersion of surface magnon shown for the 216-Å-thick, (001)-oriented Co epilayer. (a) $\theta_i = 30°$, $H \| [100]$, $\mathbf{q} \perp H$, $\lambda = 5145$ Å. The error bars on ω_S are ± 0.5 GHz. (b) $\theta_i = 60°$, $H = 1.2$ kOe, $\mathbf{q} \perp H$, $\lambda = 5145$ Å. ϕ_H denotes the in-plane angle between the crystallographic [100] direction and the external magnetic field ($\Delta\phi_H$ is $\pm 3°$). Since the in-plane anisotropy is very small, the measurements were performed at a higher resolution (< 0.1 GHz).

stant, the quantity $4\pi M + 2K_P/M$ influences the mean value of ω_S and ω_{B1} between $0 < \phi_H < 180°$. The larger error in K_P reflects the insensitivity of ω_S and ω_B to K_P because $4\pi M$ is more than a factor of 10 larger than $2K_P/M$. The same values of each of the anisotropies (K_U and K_P) are used to fit both the bulk and surface magnon in-plane dispersions (i.e., ω_S, ω_{B1}, vs ϕ_H), which is consistent with the idea that these uniaxial anisotropies are indeed bulk values. This is significant because ω_{B1} could be more sensitive to surface anisotropies than ω_S through *pinning* effects. We thus conclude that there is little evidence for surface anisotropies being different from bulk anisotropies in the (110)-oriented Co film. Figure 4 summarizes similar ω_S vs H and ω_S vs ϕ_H data from the (001)-grown Co epilayer. As in the (110)-oriented film, the frequencies for this sample also exhibit a twofold symmetry and the data reveal that the two in-plane [100] and [010] directions are magnetically inequivalent. However, since the ω_S's along these two crystallographically equivalent directions differ by only about 1 GHz, the uniaxial anisotropy is much smaller than in the (110) film. The corresponding anisotropy values deduced from fits to the Brillouin data in Fig. 4 show that K_U is indeed an order of magnitude smaller ($0.8 \pm 0.2 \times 10^5$ erg/cm^3) than that in the (110)-grown sample (see Table I). We were unable to determine K_U accurately from ω_S vs H data [Fig. 4(a)] for the surface magnon as in the (110) film because the anisotropy is much smaller for this sample. The in-plane bulk mode dispersion is not included in Fig. 4(b) for the same reason. The error in the measured bulk mode frequency is of the order of the in-plane anisotropy (1 GHz) for the (001) grown sample. The independently measured $4\pi M$ for this film was 13.5 kG. Other parameters obtained from the fits were $A = 1.9 \times 10^{-6}$ erg/cm, $\gamma = 2.02$, and $K_P = -3.7 \pm 2 \times 10^5$ erg/cm^3. We also utilized a small K_1 (-0.2×10^5 erg/cm^3) in this fit to reproduce the flattening of the in-plane dispersion evident at $0° \leq \phi_H \leq 30°$ and at $150° \leq \phi_H \leq 180°$ in Fig. 4(b).

Independent evidence for the orientation of the spontaneous axis of magnetization in each of the films was obtained by studying the directional dependence of the surface magnon. Figure 5 shows this behavior in the (110)

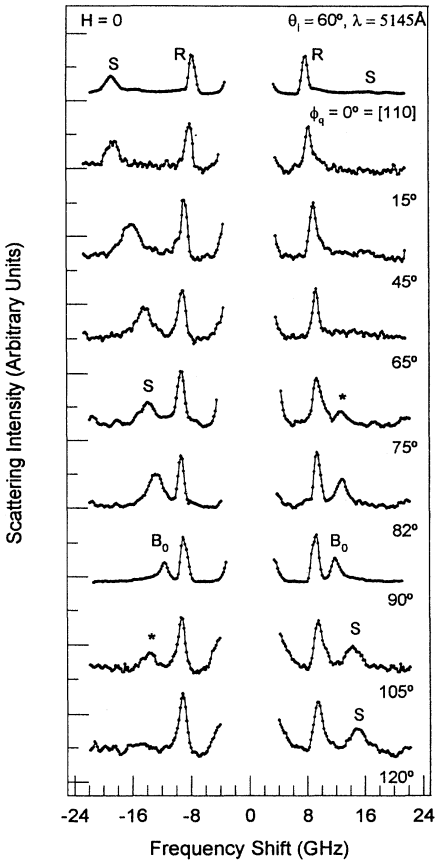

FIG. 5. In-plane dispersion, measured for $\theta_i = 60°$, $\lambda = 5145$ Å, at $H = 0$ for (110) film. The backscattered light was not analyzed so as to retain both the Rayleigh phonon (R) and the surface magnon (S). At $\phi_q = 75°$ and $\phi_q = 82°$ (direction of $\mathbf{q}$ from $[\bar{1}10]$), the intensity of the anti-Stokes spectrum (identified by an asterisk) shows a significant increase. When $\phi_q = 90°$, i.e., for $\mathbf{q}$ along [001] and parallel to $\mathbf{M}$, the surface mode peaks are replaced by two equal intensity, $n = 0$, bulk magnons (B_0) peaks.

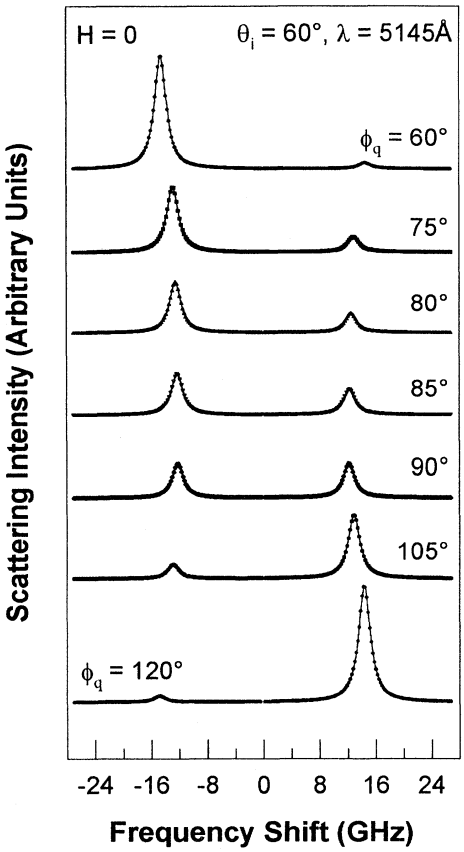

FIG. 6. Calculated Brillouin spectra for the (110)-oriented 202-Å Co film as a function of the in-plane angle ϕ_q. As $\mathbf{q}$ approaches [001] (i.e., $\phi_q \rightarrow 90°$) the Stokes–anti-Stokes ratio becomes equal, while at angles away from this direction there is a large asymmetry in the magnon intensities indicative of surfacelike behavior.

Co film at *zero* applied field. The in-plane direction of the magnon wave vector $\mathbf{q}$ is denoted by the angle ϕ_q measured from the $[\bar{1}10]$ crystal direction. When $\mathbf{q}$ is directed along $[\bar{1}10]$ ($\phi_q = 0°$), a large asymmetry is evident in the Stokes–anti-Stokes intensity ratios. However, as $\mathbf{q}$ approaches [001] ($\phi_q = 90°$), it is clear that the Stokes–anti-Stokes intensity asymmetry weakens, indicating a lack of surfacelike character. The Stokes–anti-Stokes intensity ratio shows a sudden drop around $\phi_q = 75°$, where the surface mode becomes delocalized and acquires a bulklike character. When the spin-wave propagation is parallel to the easy axis ($\mathbf{q} \| [001]$, $\phi_q = 90°$), the surface magnon transforms into the $n = 0$ bulk mode (B_0). As $\mathbf{q}$ continues to move away from [001] ($\phi_q = 105°$ and 120°), the Stokes–anti-Stokes intensity ratio switches with the Stokes peak now being the weaker of the two. The intensity of the "surface" mode at $\phi_q = 60°$ on the Stokes side is approximately the same as the intensity at $\phi_q = 120°$ on the anti-Stokes side, thus indicating that M is oriented midway at $\phi_q = 90°$ along [001].

In Fig. 6 we present calculated Brillouin spectra for this mode on the (110)-oriented Co film as a function of ϕ_q. The light-scattering intensity from a thick film has the form[17,18,21,22]

$$I = r_{yy} S_{yy}(\omega, \mathbf{q}) + r_{xx} S_{xx}(\omega, \mathbf{q}) + 2\mathrm{Re}[r_{xy} S_{xy}(\omega, \mathbf{q})] , \quad (5)$$

where the r's depend on the index of refraction, polarization, and angle of incidence of the probing electromagnetic wave. The amplitudes of the thermal spin fluctuations are given by components of the spin correlation function $S(\omega, \mathbf{q})$. Note that the r's are in general complex in the case of an absorbing medium described by a complex index of refraction. Because of this, the r_{xy} term is nonzero and responsible for a large Stokes–anti-Stokes asymmetry through the S_{xy} component of the correlation function. The spin correlation functions are constructed from the solutions $\mathbf{m}_r(\omega_r, \mathbf{q}, y)$, which satisfy the equations of motion and the associated boundary conditions

TABLE I. Summary of uniaxial anisotropies obtained from Brillouin-light-scattering experiments are magnetoelastic energy calculations. K_U and K_P are the in-plane and perpendicular uniaxial anisotropies, respectively. Other parameters extracted from the fitting procedure for the (110) film are $A=1.87\times10^{-6}$ erg/cm, $\gamma=2.02$, and $4\pi M=13$ kG. For the (001) film, $A=1.9\times10^{-6}$ erg/cm, $\gamma=2.02$. SQUID-measured values of $4\pi M$ are 13.0 and 13.5 kG in the (110) and (001) films, respectively.

Sample	Anisotropy ($\times10^5$ erg/cm^3)	Brillouin experiment	Magnetoelastic calculation
(110) film	K_U	6.2±0.5	6.7
	K_P	8.3±3.0	10.8
	K_1	0.0	NA[a]
(001) film	K_U	0.8±0.2	0.0
	K_P	−3.7±2.0	−3.1
	K_1	−0.2	NA

[a]NA: nonapplicable.

at frequency ω_r in the manner of Ref. 21, which is equivalent to the method of Ref. 22. The intensities plotted in Fig. 6 were calculated using the field parameters listed in Table I. The applied field was set to zero as in Fig. 5, and the calculated Stokes–anti-Stokes intensity ratios show the same general behavior found in the experiment.

IV. DISCUSSION

We first consider various possible contributions to the effective anisotropies used to fit the data of Figs. 2–4. The effective magnetic anisotropy energy ($K_{\rm eff}$) is in general a combination of the demagnetization (K_D), magnetocrystalline ($K_{\rm MC}$), magnetoelastic ($K_{\rm ME}$), and surface anisotropy (K_S) energies; i.e., $K_{\rm eff}=K_D+K_{\rm MC}+K_{\rm ME}+K_S$. In our convention $K_{\rm eff}$ is positive for an in-plane easy axis. The demagnetization energy for a thin film is $K_D=2\pi M^2$, where M is the magnetization per unit volume of bcc cobalt. For this calculation, the geometry is chosen so that the y axis is normal to the film plane and the z,x axes lie in plane along the easy and hard axes of magnetization, respectively. Fits to the Brillouin data reveal $K_1=0$ for the (110) film, and hence there is no contribution to $K_{\rm eff}$ from the lowest-order cubic anisotropy. Because of the relatively large thickness of our films, surface anisotropies (K_S) should not be significant. Moreover, we found no evidence for surface anisotropies in the (110) film from Brillouin fits, and hence we set $K_S=0$. Thus, in the absence of a magnetoelastic contribution, we obtain $K_{\rm eff}^{[\bar{1}10]}=K_{\rm eff}^{[001]}$. This is inconsistent with the observation of a preferential orientation of the in-plane magnetization along [001] for the (110) grown film.

A weak K_1 is present in the (001) film. However, the cubic symmetry of this term forbids a uniaxial contribution to $K_{\rm eff}$ along either principal axis in this film. Hence, in this case, also, contributions from K_S and $K_{\rm MC}$ to the free energy cannot explain the 1-GHz difference between the measured spin-wave frequencies along the two principal crystal axes. In what follows, we consider the possibility that the uniaxial anisotropies for both orientations are primarily due to magnetoelastic contributions.

We now evaluate the magnetoelastic contribution to $K_{\rm eff}$ for the (110)-oriented film along the lines followed in Refs. 6–8. The magnetoelastic energy is given by $K_{\rm ME}=-\sum_{ij}U_i^2 b_{ij}e_j$, where the b_{ij}'s are elements of the body-transformed magnetoelastic tensor, $e=(e_x,e_y,e_z)$ are the diagonal components of the strain, and $U^2=(U_x^2,U_y^2,U_z^2)$, where the U_i's are the direction cosines. We have e_y as the out-of-plane strain, while (e_z,e_x) lie in the plane of the film. The expression for the magnetoelastic strain is

$$K_{\rm ME}=-2U_y^2 b_{44}(e_y-e_x)-U_z^2\left[(b_{11}-b_{12})\left[e_z-\frac{e_x+e_y}{2}\right]+b_{44}(e_y-e_x)\right]. \tag{6}$$

Hence the coefficients of U_y^2 (U_z^2) give rise to the uniaxial anisotropies K_P (K_U). The strains are evaluated by minimizing the elastic free energy $F(e)=\frac{1}{2}\sum_{ij}e_i C_{ij}e_j$ with respect to the out-of-plane strain e_y, where $\overleftrightarrow{C}$ is the elasticity tensor in the transformed coordinate frame. On minimizing $F(e)$ we obtain

$$e_y=\left[-\frac{1}{a_{11}}\right][a_{12}e_x+c_{12}e_z], \tag{7}$$

where $a_{11}=[(C_{11}+C_{12})/2+C_{44}]$ and $a_{12}=[(C_{11}+C_{12})/2-C_{44}]$ and the C_{ij}'s are the elasticity tensor elements. Since bcc Co is closely lattice matched with the substrate, the in-plane strains arising from the predicted film-substrate lattice mismatch[3] are only $e_x\approx e_z=0.25\%$. Together with the previously measured C_{ij}'s (Ref. 14) from these *same* Co films, we hence have $e_y=-0.33\%$.

In order to estimate the magnetoelastic energy, the magnetoelastic tensor elements b_{ij} are required. Since these data are not available for bcc cobalt, we use values for fcc Co that are derived from measured magnetostriction constants λ_{100}, λ_{111} of Co-rich fcc Co/Pt alloys.[23] Beyond a concentration of 50% Co, the λ's for the alloy do not change appreciably and hence are reasonable values for the magnetostriction constants of fcc Co:

$$\lambda_{100}=-\frac{2}{3}\left[\frac{b_{11}-b_{12}}{c_{11}-c_{12}}\right],\quad \lambda_{111}=-\left[\frac{b_{44}}{3c_{44}}\right]. \tag{8}$$

Using the values of λ_{100} ($=130\times10^{-6}$), λ_{111} ($=-65\times10^{-6}$), we compute the combinations of b_{ij}'s essential to evaluate the magnetoelastic free energy and obtain $K_{\rm ME}=U_y^2(10.8\times10^5)+U_z^2(6.7\times10^5)$ erg/cm^3. $K_{\rm ME}$ thus gives rise to both an in-plane and a perpendicular anisotropy in the (110)-oriented case. The computed in-plane (coefficient of U_z^2) and out-of-plane (coefficient of U_y^2) anisotropies agree very well and the K_U and K_P values deduced from fits to the Brillouin data ($K_U=6.2\pm0.5\times10^5$ erg/cm^3 and $K_P=8.3\pm3\times10^5$ erg/cm^3, from Table I).

For the (001)-oriented film, the magnetoelastic energy is given by $K_{ME}=[U_z^2(e_x-e_z)+U_y^2(e_x-e_y)](b_{11}-b_{12})$. As before, e_y is the out-of-plane strain, while (e_z,e_x) are the in-plane strains along the easy and hard axes, respectively. We obtain $K_{ME}=U_z^2(0)+U_y^2(-3.1\times10^5)$ erg/cm^3. The corresponding results (Table I) from Brillouin scattering are $K_U=(0.8\pm0.2)\times10^5$ erg/cm^3 and $K_P=(-3.7\pm2)\times10^5$ erg/cm^3. Once again good agreement is obtained between the magnetoelastic results and fits from the Brillouin data. We note that the magnitude of K_U for the (001) film is almost an order of magnitude smaller than that for the (110) sample. This is consistent with the small (1 GHz) difference in ω_S observed in the (001) film as opposed to a larger anisotropy (6 GHz) seen in the (110) film, for **q** along the two principal in-plane directions in the respective samples. If the two in-plane strains e_x and e_z are strictly equal, there is no contribution from magnetoelastic factors to K_U for the (001)-oriented film. On the other hand, even slight differences between the in-plane strains would give rise to a finite magnetoelastic contribution, as observed in the small difference (1 GHz) between the magnon frequencies measured along the two crystallographic directions of this film. Finally, we also point out that the small value of K_U in the (001) film is equivalent to an effective interfacial anisotropy of 0.16 erg/cm^2. While this value is a reasonable estimate for a surface anisotropy in ferromagnetic thin films,[13] we are unable to determine whether K_U for the (001)-grown sample is a surface or bulk anisotropy. This is because the bulk mode data were not included in the in-plane magnon dispersion analysis [Fig. 4(b)] as the uncertainty in the measurement was comparable to the anisotropy.

We have shown that interface-driven magnetoelastic effects may account for the uniaxial anisotropies observed in the bcc Co films. Before concluding this section, we call attention to the values of magnetization used in this study. The average measured value of $4\pi M$ for the two films is about 13.2 kG, which corresponds to an average magnetic moment (μ) of about $1.3\mu_B$/atom. In contrast, the measured average magnetic moment in a thicker (357 Å) bcc Co film[3] was over $1.5\mu_B$/atom while the theoretically predicted magnetic moment is $1.7\mu_B$/atom. What causes a reduction in μ for thinner films is not clear. A recent calculation proposed that arsenic diffusion from the substrate lowers suppresses the average magnetic moment of bcc Co.[24] Evidence for a *lower* local magnetic moment per atom in bcc Co films has also been reported from neutron-scattering measurements.[25] These experiments indicated that μ varied significantly with depth within a 100-Å film. While the magnetic moment at the center agreed with the theoretically predicted value of $1.7\mu_B$ per atom, it reduced to $1.0\mu_B$ per atom at the surfaces. This yields an average of about $(1.3–1.4)\mu_B$ per atom for the entire film. If we assume that a similar reduction in magnetic moment occurs in our 200-Å-thick cobalt samples, this would account for the reduced M's measured in our samples.

V. CONCLUSION

In summary, we have measured the in-plane spin-wave dispersion in bcc cobalt epilayers of different orientations using Brillouin light scattering. In the (110)-oriented film we find a large in-plane twofold uniaxial anisotropy, while in the (001) film a similar, though much weaker, anisotropy is observed. Free energy considerations have shown that magnetoelastic interactions driven by lattice mismatch strains at the film-substrate interface, can give rise to the uniaxial anisotropy observed in the (110)-oriented epilayer. The values of the anisotropy constants deduced from these energy considerations using reasonable estimates for magnetoelastic constants and strains are found to agree with those deduced from fits to the spin-wave frequencies. The easy axis of magnetization is also directly evident by the transformation of the surface magnon into the $n=0$ bulk magnon when the magnon wave vector lies parallel to the spontaneous (easy) axis of magnetization. The much weaker uniaxial anisotropy measured for the (001)-oriented Co layer is also consistent with magnetoelastic effects, although, for exact tetragonal in-plane strain, a twofold anisotropy should be completely suppressed. The observed uniaxial anisotropy in the (001)-oriented film hence suggests that if indeed the in-plane strains are equal (i.e., $e_x=e_z$), then an additional, presently unknown, mechanism could also contribute to the small differences in the spin-wave frequencies along [100] and [010]. The need for a mechanism not related to magnetoelastic effects was suggested by recent observations of uniaxial anisotropies in $Fe_{1-x}Co_x$ alloys evident even at alloy concentrations that provided lattice match between epilayer and substrate.[26] Thus, while magnetoelastic effects likely provide the most significant contribution to magnetic anisotropies in the stabilized phase of bcc cobalt, other causes may be required to account for the residual anisotropies evident in our (001) Co film.

ACKNOWLEDGMENTS

Work at OSU was supported by the National Science Foundation under Grant No. DMR 93-03568 and that at NRL by the Office of Naval Research. R.L.S. was supported by a university seed grant.

[1]C. H. Lee, H. He, and F. Lamelas, Phys. Rev. Lett. **62**, 653 (1989).

[2]F. J. Lamelas, C. H. Lee, H. He, W. Vavra, and R. Clarke, Phys. Rev. B **40**, 5837 (1989).

[3]G. A. Prinz, Phys. Rev. Lett. **54**, 1051 (1985).

[4]C. H. Lee, R. F. C. Farrow, C. J. Liu, E. E. Marinero, and C. J. Chien, Phys. Rev. B **42**, 11 384 (1990).

[5]Brad. N. Engel, C. England, R. A. Van Leeuwen, M. H. Wied-

mann, and C. M. Falco, Phys. Rev. Lett. **67**, 1910 (1991).
[6]B. Hillebrands, J. V. Harzer, G. Guntherodt, and J. R. Dutcher, J. Magn. Soc. Jpn. **17**, 17 (1993).
[7]B. Hillebrands and J. R. Dutcher, Phys. Rev. B **47**, 6126 (1993).
[8]C. H. Lee, H. He, F. J. Lamelas, W. Vavra, C. Uher, and R. Clarke, Phys. Rev. B **42**, 1066 (1990).
[9]J. Barnas and P. Grunberg, J. Magn. Magn. Mater. **82**, 186 (1989).
[10]P. Carcia, J. Appl. Phys. **63**, 5066 (1988).
[11]G. A. Prinz, G. T. Rado, and J. Krebbs, J. Appl. Phys. **53**, 2087 (1982).
[12]U. Gradmann, J. Korecki, and G. Waller, Appl. Phys. Lett. A **39**, 101 (1986).
[13]B. Hillebrands, P. Baumgart, and G. Guntherodt, Phys. Rev. B **36**, 2450 (1987).
[14]S. Subramanian, R. Sooryakumar, G. A. Prinz, B. T. Jonker, and Y. U. Idzerda, Phys. Rev. B **49**, 17 319 (1994).
[15]R. E. Camley and D. L. Mills, Phys. Rev. B **18**, 4821 (1979).
[16]R. E. Camley and M. Grimsditch, Phys. Rev. B **22**, 5420 (1980).
[17]R. E. Camley, T. S. Rahman, and D. L. Mills, Phys. Rev. B **23**, 1226 (1981).
[18]R. E. Camley, P. Grunberg, and P. Mayr, Phys. Rev. B **26**, 2609 (1982).
[19]G. Rupp, W. Wettling, R. S. Smith, and W. Jantz, J. Magn. Magn. Mater. **45**, 404 (1984).
[20]R. L. Stamps, Phys. Rev. B **49**, 339 (1994).
[21]R. E. Camley and R. L. Stamps, in *Linear and Nonlinear Spin Waves in Magnetic Films and Superlattices,* edited by M. G. Cottam (World Scientific, Singapore, 1994), Chap. 5.
[22]J. R. Dutcher and J. F. Cochran, J. Magn. Magn. Mater. **72**, 307 (1988).
[23]H. Fujiwara, H. Kadomatsu, and T. Tokunaga, J. Magn. Magn. Mater. **31–34**, 809 (1983).
[24]D. Singh, J. Appl. Phys. **71**, 3431 (1992).
[25]J. A. C. Bland, R. D. Bateson, P. C. Riedi, R. G. Graham, H. J. Lauter, J. Penfold, and C. Shackleton, J. Appl. Phys. **69**, 4989 (1991).
[26]C. Gutierrez, J. J. Krebbs, and G. A. Prinz, Appl. Phys. Lett. **61**, 2476 (1992).